ICME09-RT-04

NONLINEAR DYNAMICS OF ELECTROSTATICALLY ACTUATED MICROSTRUCTURES UNDER THE EFFECT OF SQUEEZE FILM DAMPING

S. Chaterjee and G. Pohit

Department of Mechanical Engineering, Jadavpur University, Kolkata, India

ABSTRACT
The electrostatic force being inherently nonlinear, characterization of oscillations induced by large DC and/or AC loads is not possible with a linearized model. Moreover, electrostatic microstructures actuated by large electrostatic loads and operating in fluidic environments are subjected to nonlinear damping. Under the effect of these nonlinearities, electrostatic MEMS exhibit interesting dynamic characteristics. A reduced order model (ROM) of an electrically actuated microcantilever formulated accounting for the nonlinearities of the system is numerically simulated to observe the nonlinear dynamics. The presented model and methodology enable simulation of the transient as well as the steady-state dynamics for slip flow conditions. Nonlinear phenomena such as softening, nonlinear resonance, superharmonic resonance of second order, and dynamic pull-in are predicted. Squeeze film damping is found to considerably affect the observed nonlinear phenomena.

Keywords: MEMS, Squeeze Film Damping, Superharmonic Resonance, Dynamic Pull-In.

1. INTRODUCTION

The coupled electrical-mechanical nature of electrostatic MEMS gives rise to interesting dynamic characteristics of these devices [1-4] which can have significant impact in their applications as capacitive switches, resonators, tunable capacitors, and actuators. The electrostatic MEMS devices are inherently nonlinear due to the nonlinear nature of the electrostatic forces [5]. Manifestations of this nonlinearity have resulted in various nonlinear phenomena like pull-in instabilities [6-10], jump phenomenon and hysteresis [10, 11], superharmonic [12, 13] and subharmonic [11, 13] resonances, period-doubling bifurcations [10-12], and chaos [12]. Moreover, the damping of electrically actuated microstructures vibrating in presence of fluid trapped in the narrow gap between deformable and fixed electrodes is dominated by nonlinear squeeze film damping [14] and needs to be taken into account for effective simulation of the system dynamics. Several approaches to model and numerically simulate these nonlinear devices have been reported in open literature. In [6, 7], MEMS dynamics were investigated for purely DC loads under damped operating conditions. Purely DC loads and undamped operating conditions were dealt in [8, 9]. Effects of electrostatic actuation by a combination of DC and AC loads in presence of linear viscous damping were studied in [10, 11, and 13]. Full-Lagrangian based relaxation and Newton schemes were presented in [12] for dynamic analysis of nonlinearly damped electrostatic MEMS devices. Few studies in the existing literature deal with a unified yet simple model to successfully tackle the varying range of loading and damping conditions.

In this paper, numerically simulated dynamics of electrostatic microcantilevers actuated by purely DC load or a combination of DC and AC loads, and, operated under damped or undamped conditions are investigated and comparisons are drawn. A reduced order model (ROM) formulated accounting for the nonlinearities of the system, arising out of electric forces and the damping terms, is successfully employed to predict the nonlinear dynamics. Squeeze film damping is found to considerably affect the observed nonlinear phenomena.

2. GOVERNING EQUATIONS

The model (Fig 1) shows a damped cantilever beam of length l, width b, thickness h separated from the ground plane by a small initial air-gap of d_0.
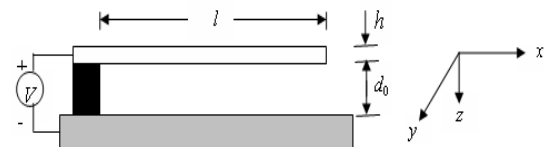

Fig 1. A schematic diagram of an electrostatically actuated microcantilever beam model.

When subjected to a driving voltage $V(t)$ comprising of a DC voltage V_{DC} and an AC component $V_{AC} \cos(\omega t)$, the beam undergoes oscillatory motions

and these oscillations redistribute pressure in the air trapped in the non-uniform gap spacing causing a damping effect. Let $w(x,t)$ denote the transverse displacement of the beam being dependent on the position x along the beam length and time t. Following the elastic beam theory, and, adding terms representing electrostatic excitation and squeeze film effect, the governing equation of the one-dimensional Euler-beam for small air gap is given by

$$\rho A \frac{\partial^2 w}{\partial t^2} + EI \frac{\partial^4 w}{\partial x^4} = \frac{1}{2} \frac{\varepsilon_0 b V^2}{(d_0 - w)^2} - f_d(x,t) \qquad (1a)$$

with the boundary conditions as

$$w(0,t) = \frac{\partial w}{\partial x}\bigg|_{x=0} = 0,$$

$$\frac{\partial^2 w}{\partial x^2}\bigg|_{x=l} = \frac{\partial^3 w}{\partial x^3}\bigg|_{x=l} = 0 \qquad (1b)$$

where ρ is the density of the beam material; permittivity constant for free space $\varepsilon_0 = 8.854 \times 10^{-12}, Fm^{-1}$; plate modulus for wide beams $E = E'/(1-v^2)$, E' is the Young's modulus, v is the Poisson's ratio. The beam is assumed to be prismatic with rectangular cross section, thereby the moment of inertia and the area of the cross section can be given by $I = bh^3/12$ and $A = bh$, respectively. The first term on the right hand side of Eq. (1a) represents the excitation force per unit length while the second term represents the force acting on the beam owing to the pressure of the squeezed gas film between the beam and the ground plane.

The one-dimensional force due to squeeze film damping is obtained by integrating the two-dimensional pressure distribution along the width of the beam, and, is given by

$$f_d(x,t) = \int_0^b \left[p(x,y,t) - p_a \right] dy \qquad (2)$$

where $p(x,y,t)$ is the absolute pressure in the gap and p_a is the ambient pressure. For slow viscous motion within small gaps and the motion of the beam being restricted to normal approach, the pressure $p(x,y,t)$ is governed by the nonlinear Reynolds equation [14]

$$\frac{\partial}{\partial x}\left(\frac{\rho_a g^3}{12\mu} \frac{\partial p}{\partial x} \right) + \frac{\partial}{\partial y}\left(\frac{\rho_a g^3}{12\mu} \frac{\partial p}{\partial y} \right) = \frac{\partial}{\partial t}(\rho_a g) \qquad (3a)$$

with the trivial boundary conditions, applicable for small air-gaps, as

$$p(x,0,t) = p(x,b,t) = p(l,y,t) = p_a, \text{ and,}$$

$$\frac{\partial p(0,y,t)}{\partial x} = 0 \qquad (3b)$$

where ρ_a is the density of ambient air; the non-uniform gap spacing $g(x,t) = d_0 - w(x,t)$; μ is the dynamic viscosity of air under standard temperature and pressure.

Assuming the flow to be incompressible, and, considering an effective air viscosity μ_{eff} [14] to take into account the slip-flow conditions, Eq. (3a) can be reduced to

$$\frac{\partial}{\partial x}\left(g^3 \frac{\partial p}{\partial x} \right) + \frac{\partial}{\partial y}\left(g^3 \frac{\partial p}{\partial y} \right) = 12\mu_{eff} \frac{\partial g}{\partial t} \qquad (4)$$

where effective viscosity $\mu_{eff} = \mu/(1+6Kn)$, calculated using Burgdorfer's model; Knudsen number $Kn = \lambda_a/g$; $\lambda_a = \lambda_0 p_0/p_a$ is the mean free path at ambient pressure p_a. The mean free path λ_0 at standard temperature and pressure $p_0 = 1.013 \times 10^5, Pa$ conditions is about $65 \times 10^{-9}, m$. Using Eq. (2) and the nondimensional variables $\bar{x} = x/l, \bar{y} = y/b$, $\bar{w} = w/d_0, \bar{g} = g/d_0$, $\bar{p} = p/p_a$, $\bar{t} = t/s$, $s = l^2(\sqrt{\rho A}/\sqrt{EI})$, Eq. (1) and Eq. (4) can be expressed as

$$\frac{\partial^2 \bar{w}}{\partial \bar{t}^2} + \frac{\partial^4 \bar{w}}{\partial \bar{x}^4} = \frac{\alpha_2 V^2}{(1-\bar{w})^2} - \hat{P} \int_0^1 (\bar{p} - 1) d\bar{y} \qquad (5a)$$

$$\bar{w}(0,\bar{t}) = \frac{\partial \bar{w}}{\partial \bar{x}}\bigg|_{\bar{x}=0} = 0,$$

$$\frac{\partial^2 \bar{w}}{\partial \bar{x}^2}\bigg|_{\bar{x}=1} = \frac{\partial^3 \bar{w}}{\partial \bar{x}^3}\bigg|_{\bar{x}=1} = 0, \qquad (5b)$$

and

$$\left(\frac{d_0}{l}\right)^2 \frac{\partial}{\partial \bar{x}}\left(\bar{g}^3 \frac{\partial \bar{p}}{\partial \bar{x}} \right) + \left(\frac{d_0}{b}\right)^2 \frac{\partial}{\partial \bar{y}}\left(\bar{g}^3 \frac{\partial \bar{p}}{\partial \bar{y}} \right)$$

$$= \frac{12\mu_{eff}}{p_a \, s} \frac{\partial \bar{g}}{\partial \bar{t}} \qquad (6a)$$

respectively, where $\alpha_2 = (1/2)(\varepsilon_0 bl^4/EId_0^3)$, $\hat{P} = l^4 bp_a/EId_0$, $V(\bar{t}) = V_{DC} + V_{AC} \cos(s\omega \bar{t})$; with the pressure boundary conditions, Eq. (3b), can be rewritten as

2

$$\overline{p}(\overline{x},0,\overline{t}) = \overline{p}(\overline{x},1,\overline{t}) = \overline{p}(1,\overline{y},\overline{t}) = 1, \ \frac{\partial \overline{p}(0,\overline{y},\overline{t})}{\partial \overline{x}} = 0$$

$$(6b)$$

Taking into consideration the boundary conditions, Eq. (6b), absolute pressure underneath the vibrating plate can be written as

$$\overline{p}(\overline{x},\overline{y},\overline{t}) = 1 + P^{*}(\overline{x},\overline{y},\overline{t}) \qquad (7)$$

where $P^{*}(\overline{x},\overline{y},\overline{t}) = \psi(\overline{x})(\overline{y} - \overline{y}^{2})e^{j(s\omega)\overline{t}}$ is used assuming, as in earlier works [6, 7], the spatial distribution of pressure to be separable being the product of a parabolic function along the beam width and an unknown function $\psi(\overline{x})$ along the beam length.

Substituting Eq. (7) in Eq. (6a) and integrating the resulting equation across the width of the beam leads to

$$\left(\frac{d_0}{l}\right)^2 \frac{1}{2} \overline{g}^2 \frac{\partial \overline{g}}{\partial \overline{x}} \frac{\partial \psi}{\partial \overline{x}} e^{j(s\omega)\overline{t}} + \left(\frac{d_0}{l}\right)^2 \frac{1}{6} \overline{g}^3 \frac{\partial^2 \psi}{\partial \overline{x}^2}$$

$$e^{j(s\omega)\overline{t}} - \left(\frac{d_0}{b}\right)^2 2\overline{g}^3 \psi e^{j(s\omega)\overline{t}} = \frac{12\mu_{eff}}{p_a \ s} \frac{\partial \overline{g}}{\partial \overline{t}} \qquad (8)$$

For air-gap to length ratio d_0/l less than 0.3 [9], the $(d_0/l)^2$ terms in the expression for the electrostatic force [9] can be safely neglected. As expressed in Eq. (1a), the present model neglects the $(d_0/l)^2$ terms in the expression for the electrostatic force and thus assumes parallel plate capacitance. For compatibility of the fluid model with the electrostatic model, the $(d_0/l)^2$ terms in Eq. (8) are neglected to obtain the pressure function $\psi(\overline{x})$ as

$$\psi(\overline{x}) = \frac{6\mu_{eff}b^2}{d_0^2 \ p_a} \frac{1}{s} \frac{1}{(1-\overline{w})^3} \frac{\partial \overline{w}}{\partial \overline{t}} e^{-j(s\omega)\overline{t}} \qquad (9)$$

Using Eqs. (7) and (9), Eq. (5a) can be rewritten as

$$\frac{\partial^2 \overline{w}}{\partial \overline{t}^2} + \frac{\partial^4 \overline{w}}{\partial \overline{x}^4} = \frac{\alpha_2 V^2}{(1-\overline{w})^2} - \frac{\gamma}{(1-\overline{w}+6\overline{\lambda})(1-\overline{w})^2} \frac{\partial \overline{w}}{\partial \overline{t}}$$

$$(10)$$

where $\gamma = (\mu l^2 / \sqrt{EI\rho A})(b/d_0)^3$; $\overline{\lambda} = \lambda_a/d_0$. The second term on the right hand side of Eq. (10) is proportional to the beam velocity with the coefficient being a nonlinear function of the beam displacement.

3. REDUCED ORDER MODEL (ROM)

The method of Galerkin decomposition is employed to approximate the system Eq. (10) by a reduced order model composed of a finite number of discrete modal equations. The process of Galerkin decomposition starts

with separating the dependences of the deflection of the deformed beam, $\overline{w}(\overline{x},\overline{t})$, into temporals and spatials by functions $a_i(\overline{t})$ and $\phi_i(\overline{x})$ respectively, in the form of a series of products, i.e.,

$$\overline{w}(\overline{x},\overline{t}) = \sum_{i=1}^{N} a_i(\overline{t})\phi_i(\overline{x}) \qquad (11)$$

where N represents the number of modes retained in the solution. $\phi_i(\overline{x})$ is the ith linear undamped mode shape of the undeflected microcantilever obtained from the following linear undamped eigenvalue problem of a straight beam

$$\frac{d^4 \phi_i}{d\overline{x}^4} = (s\omega_i)^2 \phi_i \qquad (12a)$$

$$\phi_i(0) = \frac{d\phi_i}{d\overline{x}}\bigg|_{\overline{x}=0} = \frac{d^2\phi_i}{d\overline{x}^2}\bigg|_{\overline{x}=1} = \frac{d^3\phi_i}{d\overline{x}^3}\bigg|_{\overline{x}=1} = 0 \qquad (12b)$$

It is worth mentioning that $\phi_i(\overline{x})$ is normalized such that $\int_0^1 \phi_i^2 d\overline{x} = 1$.

Multiplying Eq. (10) by $(1-\overline{w}+6\overline{\lambda})(1-\overline{w})^2$, substituting Eq. (11) and (12a) into the resulting equation, multiplying by $\phi_n(\overline{x})$, and integrating the outcome from $\overline{x}=0$ to 1, the set of coupled nonlinear algebraic equations can be derived as

$$(1+6\overline{\lambda})\frac{\partial^2 a_n}{\partial \overline{t}^2} + \gamma \frac{\partial a_n}{\partial \overline{t}} + \left[(1+6\overline{\lambda})(s\omega_n)^2 + \alpha_2 V^2\right]a_n$$

$$-(3+12\overline{\lambda})\sum_{i=1}^{N}\sum_{j=1}^{N}\frac{\partial^2 a_i}{\partial \overline{t}^2}a_j\int_0^1 \phi_n\phi_i\phi_j d\overline{x} - (3+12\overline{\lambda})$$

$$\sum_{i=1}^{N}\sum_{j=1}^{N}a_ia_j(s\omega_i)^2\int_0^1 \phi_n\phi_i\phi_j d\overline{x} + (3+6\overline{\lambda})\sum_{i=1}^{N}\sum_{j=1}^{N}\sum_{k=1}^{N}\frac{\partial^2 a_i}{\partial \overline{t}^2}$$

$$a_ja_k\int_0^1 \phi_n\phi_i\phi_j\phi_k d\overline{x} + (3+6\overline{\lambda})\sum_{i=1}^{N}\sum_{j=1}^{N}\sum_{k=1}^{N}a_ia_ja_k(s\omega_i)^2$$

$$\int_0^1 \phi_n\phi_i\phi_j\phi_k d\overline{x} - \sum_{i=1}^{N}\sum_{j=1}^{N}\sum_{k=1}^{N}\sum_{p=1}^{N}\frac{\partial^2 a_i}{\partial \overline{t}^2}a_ja_ka_p$$

$$\int_0^1 \phi_n\phi_i\phi_j\phi_k\phi_p d\overline{x} - \sum_{i=1}^{N}\sum_{j=1}^{N}\sum_{k=1}^{N}\sum_{p=1}^{N}a_ia_ja_ka_p(s\omega_i)^2$$

$$\int_0^1 \phi_n\phi_i\phi_j\phi_k\phi_p d\overline{x} - (1+6\overline{\lambda})\alpha_2 V^2\int_0^1 \phi_n d\overline{x} = 0,$$

$$n = 1, 2, ..., N \qquad (13)$$

4. RESULTS

The entire analysis is carried out using the ROM retaining five ($N = 5$) modes in Eq. (13). As shown in earlier work [9], at least five modes are required to correctly simulate the pull-in instabilities using reduced order models. The dynamic analysis is carried out by numerically solving the set of nonlinear ODEs obtained retaining five (N = 5) modes in Eq. (13).Static analysis can be done by numerically solving the set of nonlinear algebraic equations obtained from Eq. (13) with $a_i(\bar{t})$ being let independent of time, V_{AC} equal to zero, and all the time derivatives set equal to zero. The design properties used in the present analysis are $l = 150\,\mu m$, $b = 22\,\mu m$, $h = 4\,\mu m$, $d_0 = 1.4\,\mu m$, $E = 160e9\,Pa$, $\rho = 2330\,kg/m^3$, $p_a = 1.013e5\,Pa$, $\mu = 1.8e - 5\,Ns/m^2$ as used in [15].

The present procedure has been validated by comparing the numerical results with the experimental results of [15]. For the above mentioned design properties of the beam, experiments were carried out in [15] to extract the damping ratio under excitation voltage ($V_{DC} + V_{AC}$) in the range of 10% to 20% of the static pull-in voltage [9]. The experimentally obtained first resonance frequency was reported to be $240\,kHz$. To facilitate comparison, the present numerical simulation is carried out for V_{DC} equal to $5V$ and V_{AC} equal to $1V$ with the excitation voltage ($V_{DC} + V_{AC}$) about 14% of the static pull-in voltage ($41.94\,V$). As shown in Fig 2, the resonance frequency is obtained to be $236\,kHz$ which is very close to the experimental observation of [15].
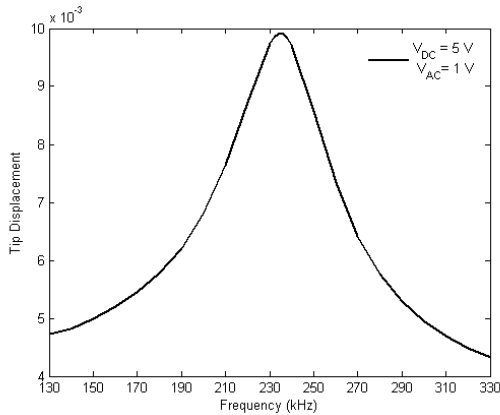

Fig 2. Frequency response curve.

Next, the microcantilever is subjected to purely DC (V_{DC}) load and the transient dynamics is investigated for both damped and undamped conditions. For the undamped case, periodic motion is observed (Figs 3 & 4) below a certain critical value of the voltage known as the dynamic pull-in voltage (V_{DPI}).
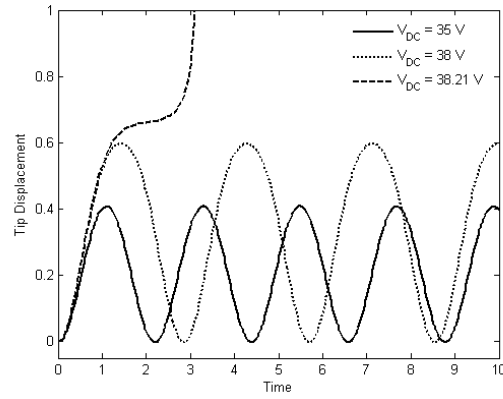

Fig 3. Undamped deflection time history.

Increase in time period (Fig 3) with V_{DC} indicates softening effect of electrostatic nonlinearity. As V_{DC} is increased to V_{DPI} ($38.21V$), the motion diverges and the beam abruptly collapses onto the electrode.
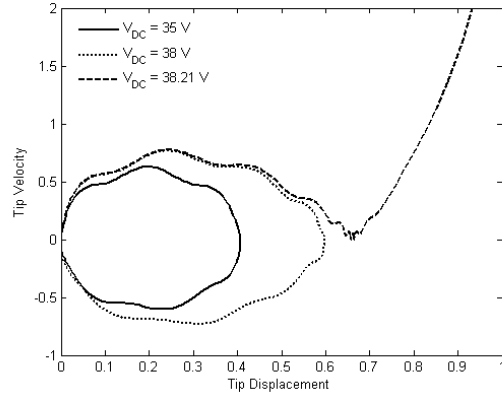

Fig 4. Undamped phase plot.

In interpreting the results in Figs 3 & 4, it may be noted that the normalized tip displacement equal to unity corresponds to collapse of the cantilever into the fixed electrode.
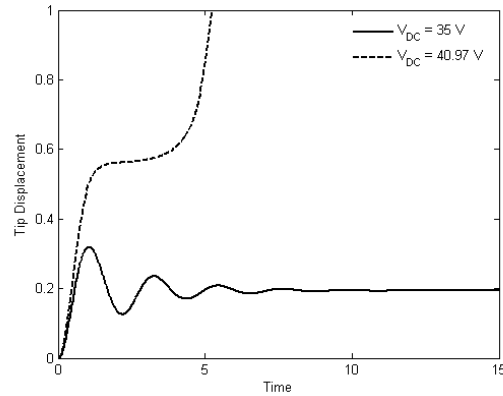

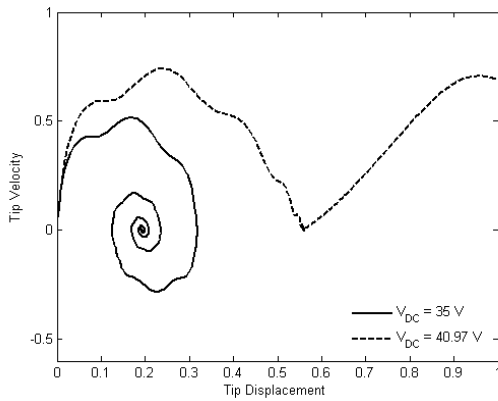Fig 5. Damped deflection time history.

Fig 6. Damped phase plot.

Under squeeze film damping, the beam performs a decaying oscillatory (Figs 5 & 6) motion for V_{DC} below the damped dynamic pull-in voltage (V_{DDPI}), and, finally settles to a steady deformed state. V_{DDPI} ($40.97\,V$) has been observed to be higher than V_{DPI} ($38.21\,V$) and approaches the static pull-in voltage ($41.94\,V$). The pull-in displacement for the undamped case ($0.6 - 0.7$) is found to be higher than for the damped case ($0.5 - 0.6$), thus shrinking the region of stability. The separatrix on the phase plane (Figs 4 & 6) separates the stable and unstable regions.
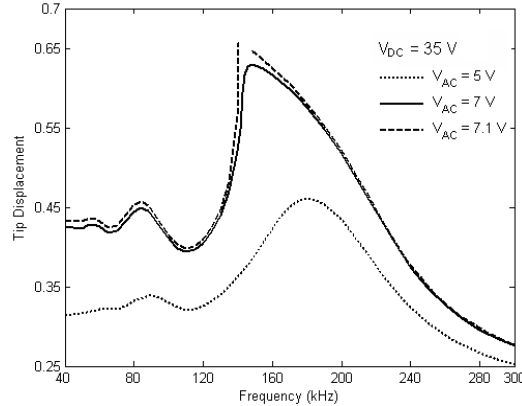

Fig 7. Frequency response curve.

The nonlinear dynamic behaviour is then studied for combined DC and AC loads in the primary and superharmonic frequency range. Frequency-response curve (Fig 7) obtained for a certain DC bias and varying AC amplitudes shows primary as well as possible existence of second order superharmonic resonances. With increase in V_{AC}, the resonant peaks shift towards the left indicating softening behaviour. As shown in Fig 7, the dynamic pull-in is observed at V_{DC} equal to $35\,V$ and V_{AC} equal to $7.1\,V$ for which the left and right branches of the frequency-response curve do not close-in and both the branches terminate as normalized

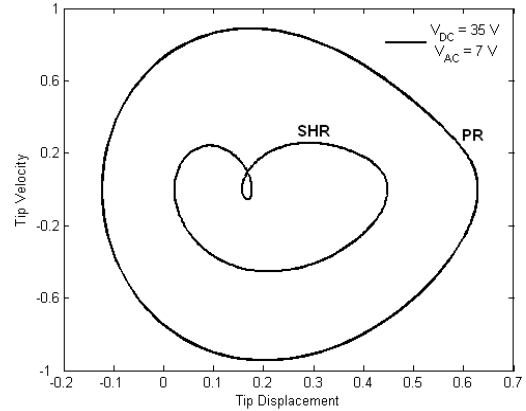tip displacement exceeds 0.65.

Fig 8. Phase plot at resonance.

Fig 8 shows the phase plot for primary (PR) as well as superharmonic (SHR) resonances just before dynamic pull-in. When actuated by a combination of DC and AC loads, dynamic pull-in of the cantilever beam occurs at a much lower V_{DC} ($35\,V$) (Fig 7) than when actuated by a purely DC (V_{DC} equal to $40.97\,V$) (Fig 5) load.

5. CONCLUSION

Nonlinear phenomena of resonance shift, superharmonic resonance, and dynamic pull-in associated with electrostatic MEMS have been presented in this paper. The present model is valid for incompressible flow in the slip flow regime. The nonlinear electrostatic force is found to be responsible for the nonlinear dynamic properties observed while the nonlinear damping force influences a quantitative shift in the design parameters like time period, oscillation amplitude, dynamic pull-in voltage and pull-in displacement. The present approach enables selection of DC bias and the amplitude and frequency of harmonic AC loading for realization of both pull-in and non-pull-in devices.

6. REFERENCES

1. Gaillard, J., Skove, M. J., Ciocan, R. and Rao, A. M., 2006, "Electrical detection of oscillations in microcantilevers and nanocantilevers", Review of Scientific Instruments, 77: 073907.
2. Zhao, J. P., Chen, H. L., Huang, J. M. and Liu, A. Q., 2005, "A study of dynamic characteristics and simulation of MEMS torsional micromirrors", Sensors and Actuators A, 120: 199–210.
3. Jin, Z. and Yang, Y., 1998, "Electrostatic resonator with second superharmonic resonance", Sensors and Actuators A, 64: 273-279.
4. Fischer, M., Giousouf, M., Schaepperle, J., Eichner, D., Weinmann, M., von Miinch, W. and Assmus, F., 1998, "Electrostatically deflectable polysilicon micromirrors – dynamic behaviour and comparison with the results from FEM modeling with ANSYS", Sensors and Actuators A, 67: 89-95.

5. Pelesko, J.A. and Bernstein, D.H., 2003, *Modeling MEMS and NEMS (Chapter 7)*, Chapman&Hall/CRC Press, London/New York/Washington, DC.
6. McCarthy, B., Adams, G., McGruer, N. and Potter, D., 2002, "A dynamic model, including contact bounce, of an electrostatically actuated microswitch", Journal of Microelectromechanical Systems, 11: 276–283.
7. Krylov, S. and Maimon, R., 2004, "Pull-in dynamics of an elastic beam actuated by continuously distributed electrostatic force", Journal of Vibration and Acoustics, 126: 332–342.
8. Xie, W.C., Lee, H.P. and Lim, S.P., 2003, "Nonlinear dynamic analysis of MEMS switches by nonlinear modal analysis", Nonlinear Dynamics, 31: 243–256.
9. Chaterjee, S. and Pohit, G., 2009, "A large deflection model for the pull-in analysis of electrostatically actuated microcantilever beams", Journal of Sound and Vibration, 322: 969-986.
10. Nayfeh, A. H., Younis, M. I. and Abdel-Rahman, E. M., 2007, "Dynamic pull-in phenomenon in MEMS resonators", Nonlinear Dynamics, 48: 153–163.
11. Mestrom, R.M.C., Fey, R.H.B., van Beek, J.T.M., Phan, K.L. and Nijmeijer, H., 2008, "Modelling the dynamics of a MEMS resonator: Simulations and experiments", Sensors and Actuators A, 142: 306–315.
12. De, S. K. and Aluru, N. R., 2006, "Complex nonlinear oscillations in electrostatically actuated microstructures", Journal of Microelectromechanical Systems, 15: 355-369.
13. Nayfeh, A. H. and Younis, M. I., 2005, "Dynamics of MEMS resonators under superharmonic and subharmonic excitations", Journal of Micromechanics and Microengineering, 15: 1840–1847.
14. Bao, M. and Yang, H., 2007, "Review of squeeze film air damping in MEMS", Sensors and Actuators A 136: 3–27.
15. Pandey, A. K. and Pratap, R., 2007, "Effect of flexural modes on squeeze film damping in MEMS cantilever resonators", Journal of Micromechanics and Microengineering 17: 2475–2484.

7. NOMENCLATURE

Symbol	Meaning	Unit
l	Beam length	μm
b	Beam width	μm
h	Beam thickness	μm
d_0	Air-gap	μm
x	Length co-ordinate	μm
y	Width co-ordinate	μm
t	Time	sec
$V(t)$	Excitation voltage	V
V_{DC}	DC voltage	V
V_{AC}	AC voltage	V
ω	Excitation frequency	rad/s
w	Beam displacement	μm
ρ	Density of beam material	Kg/m^3
f_d	Damping force	N/m
ε_0	Permittivity constant for free space	F/m
E	Plate modulus	N/m^2
E'	Young's modulus	N/m^2
ν	Poisson's ratio	-
I	Area moment of inertia	m^4
A	Cross sectional area	m^2
p	Absolute pressure	P_a
p_a	Ambient pressure	P_a
ρ_a	Density of ambient air	Kg/m^3
g	Non-uniform gap spacing	μm
μ	Coefficient of viscosity	Ns/m^2
μ_{eff}	Effective coefficient of viscosity	Ns/m^2
Kn	Knudsen number	-
λ_a	Mean free path at ambient pressure	m
α_2	Strength of electric actuation	-
$\hat{P}$	Non-dimensional pressure	-
P^*	Pressure variation	-
ψ	Pressure function	-
γ	Damping factor	-

8. MAILING ADDRESS

S Chaterjee
Department of Mechanical Engineering, Jadavpur University, Kolkata 700032, India.
Email: gpohit@vsnl.net
Telefax: +91 33 2414 6890)